

Electronic Supplementary Material

Self-assembled monolayer modulated Plateau-Rayleigh instability and enhanced chemical stability of silver nanowire for invisibly patterned, stable transparent electrodes

Gui-Shi Liu¹, Huajian Zheng¹, Zijie Zeng¹, Yexiong Wang¹, Weidong Guo¹, Ting Wang³, Heng Chen¹, Yunsen Chen¹, Shiqi Hu¹, Lei Chen¹, Yaofei Chen¹, Weiguang Xie², Bo-Ru Yang³(✉), and Yunhan Luo¹(✉)

¹ Guangdong Provincial Key Laboratory of Optical Fiber Sensing and Communications, Key Laboratory of Visible Light Communications of Guangzhou, Key Laboratory of Optoelectronic Information and Sensing Technologies of Guangdong Higher Education Institutes, Department of Optoelectronic Engineering, Jinan University, Guangzhou 510632, China

² Siyuan Laboratory, Guangzhou Key Laboratory of Vacuum Coating Technologies and New Energy Materials, Department of Physics, Jinan University, Guangzhou 510632, China

³ State Key Laboratory of Optoelectronic Materials and Technologies, School of Electronics and Information Technology, Sun Yat-sen University, Guangzhou 510006, China

Supporting information to <https://doi.org/10.1007/s12274-021-4042-3>

Supporting Figures

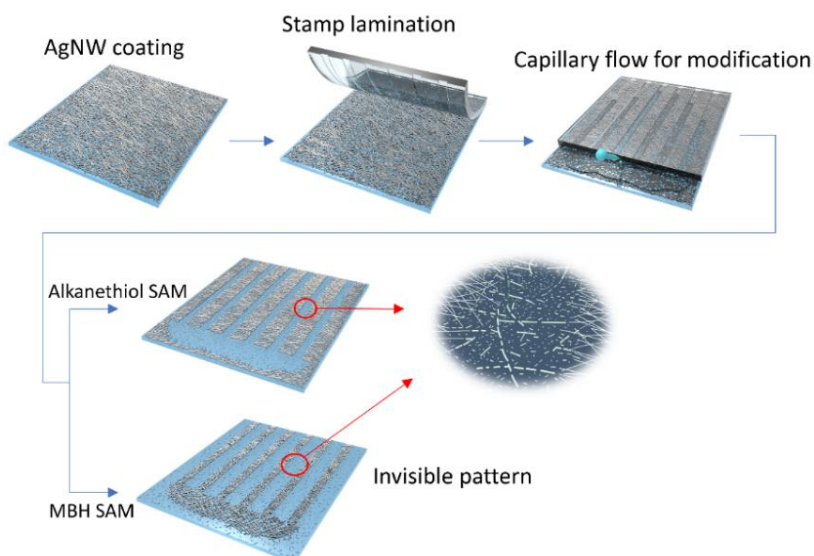


Figure S1. Schematic illustration of the selective modification with stamp-induced capillary flow.

Address correspondence to BoRu Yang, paulyang68@icloud.com; Yunhan Luo, yunhanluo@163.com

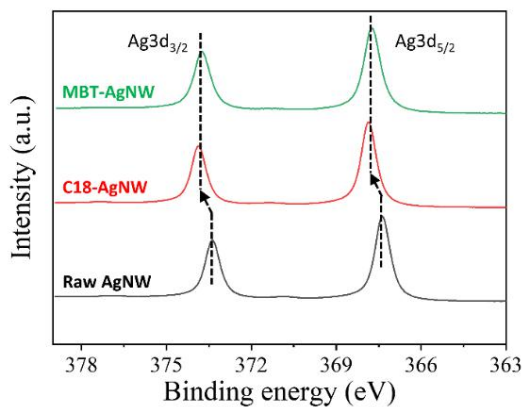


Figure S2. High-resolution XPS spectra of Ag3d for raw AgNWs, C18-AgNWs, and MBT-AgNWs. The binding energy of $\text{Ag3d}_{3/2}$ shifts from 373.38 eV to 373.88 eV after C18 modification and 373.78 eV after MBT modification. The binding energy of $\text{Ag3d}_{5/2}$ shifts from 367.38 eV to 367.88 eV after C18 modification and 367.73 eV after MBT modification.

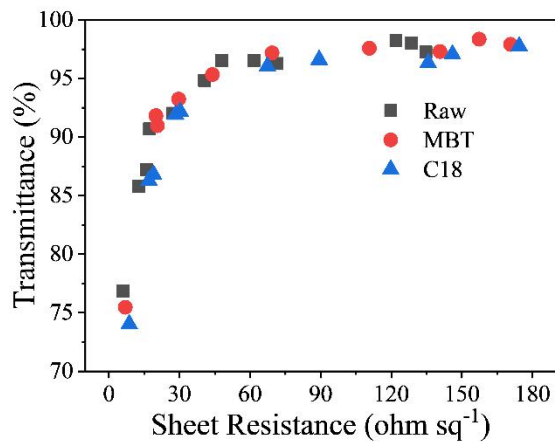


Figure S3. Plot of R_s versus transmittance at 550 nm for raw AgNW, C18-AgNW, and MBT-AgNW.

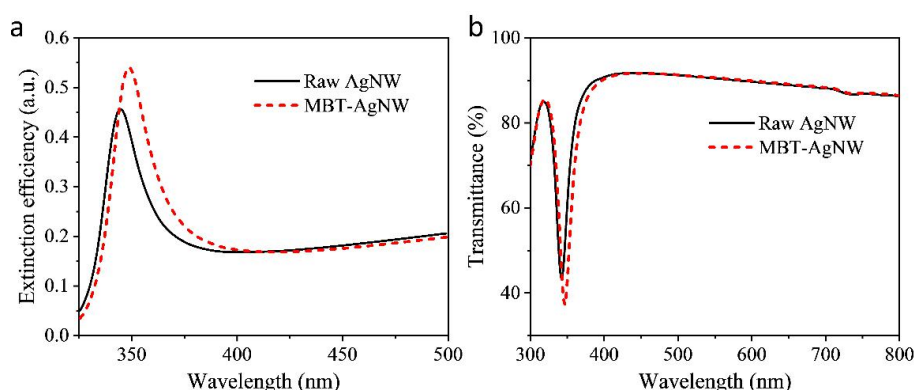


Figure S4. FDTD simulation of (a) extinction efficiency and (b) transmittance spectra of raw AgNW and MBT-AgNW, the nanowire diameter is 30 nm and the SAM thickness is set as 1.5 nm.

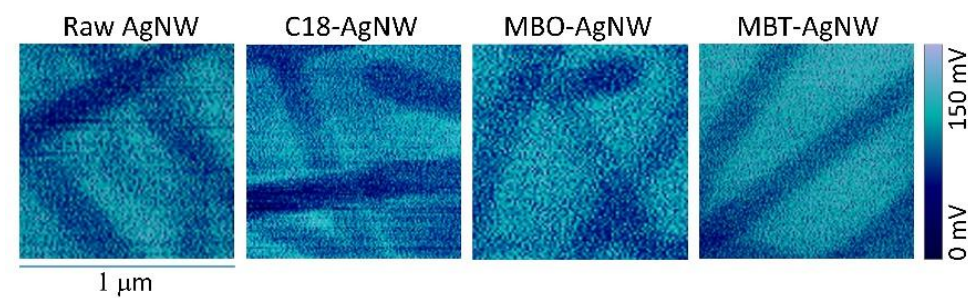


Figure S5. Surface potential images of raw AgNW, C18-AgNW, MBO-AgNW, and MBT-AgNW networks on silicon substrates.

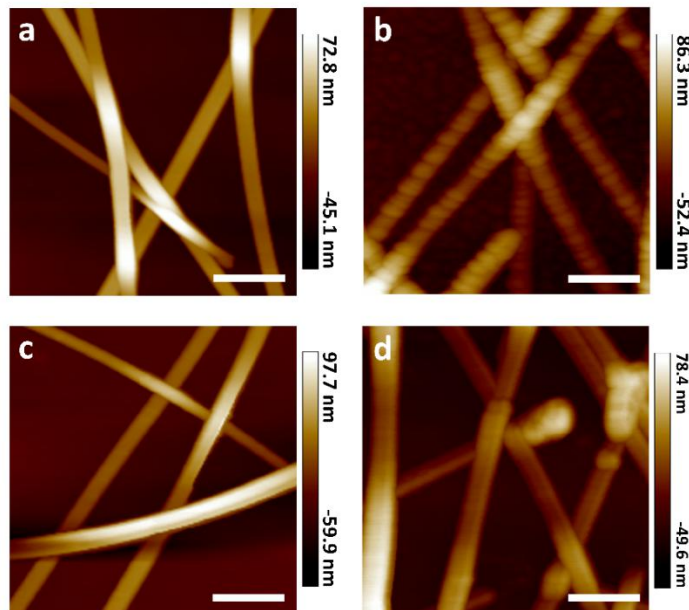


Figure S6. Atomic force images of (a) raw-AgNW, (b) C18-AgNW, (c) MBT-AgNW, and (d) MBO-AgNW.

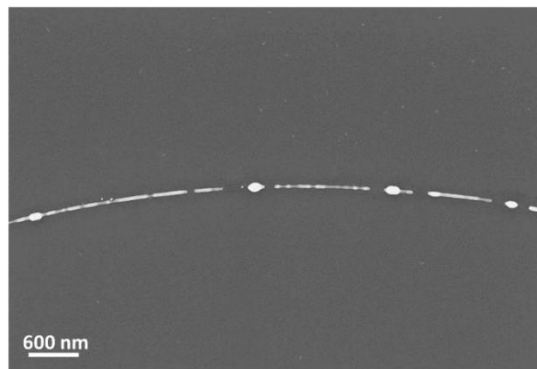


Figure S7. SEM image of the C18-AgNW after thermal annealing, showing periodic aggregations on the nanowire.

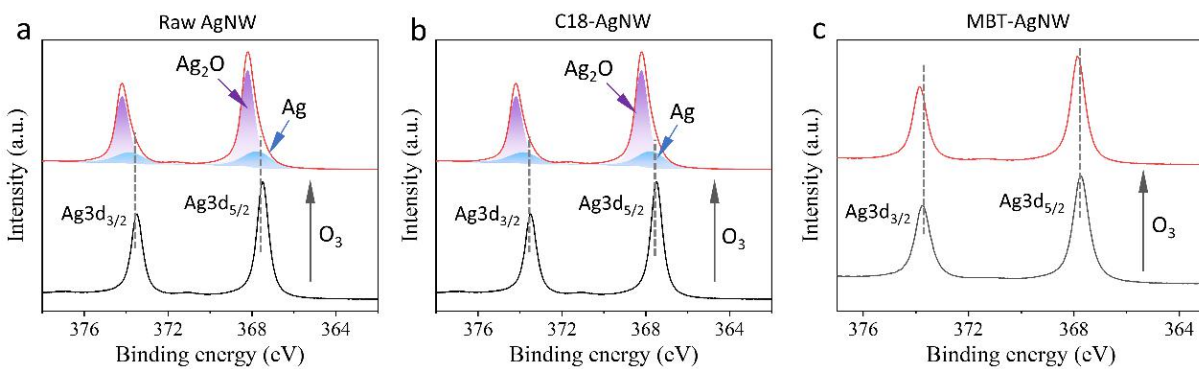


Figure S8. Ag3d XPS spectra of the (a) raw AgNWs, (b) C18-AgNWs and (c) MBT-AgNW before and after the oxidation treatment with 10k ppm for 1 hour. The XPS peaks of $\text{Ag}3\text{d}_{3/2}$ and $\text{Ag}3\text{d}_{5/2}$ shift to higher binding energies (E_b) from (373.48, 367.48 eV) to (374.18, 368.18 eV) for the raw AgNWs and (373.85, 367.85 eV) to (374.41, 368.41 eV) for the MBT-AgNWs after the oxidation treatment, respectively.

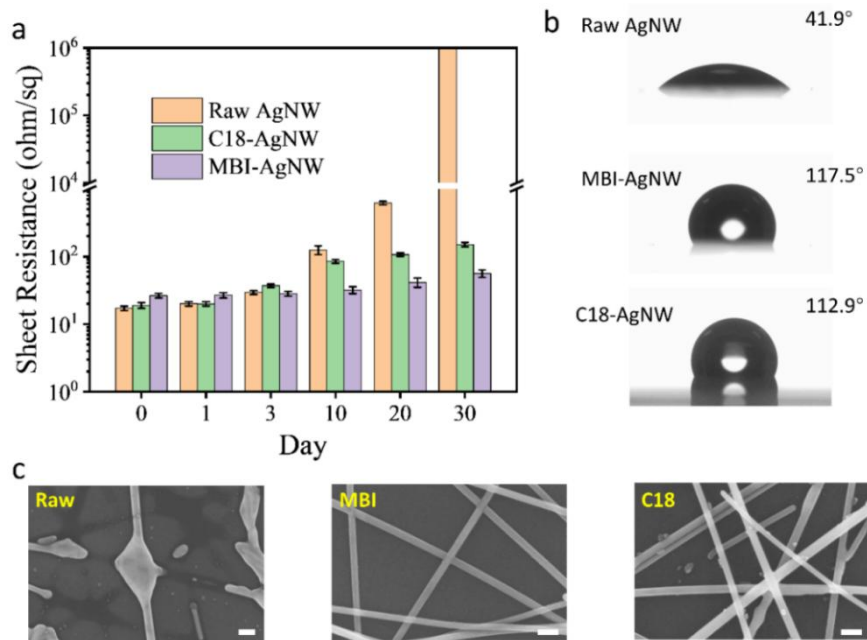


Figure S9. (a) Variation in sheet resistance of raw AgNWs, C18-AgNWs, and MBI-AgNWs under a one-month accelerated aging test of 85 °C and 85% relative humidity. (b) Water contact angles of raw AgNW, C18-AgNW, MBI-AgNW networks on glass substrates. (c) SEM images of raw AgNWs MBI-AgNWs, and C18-AgNWs after the aging test.

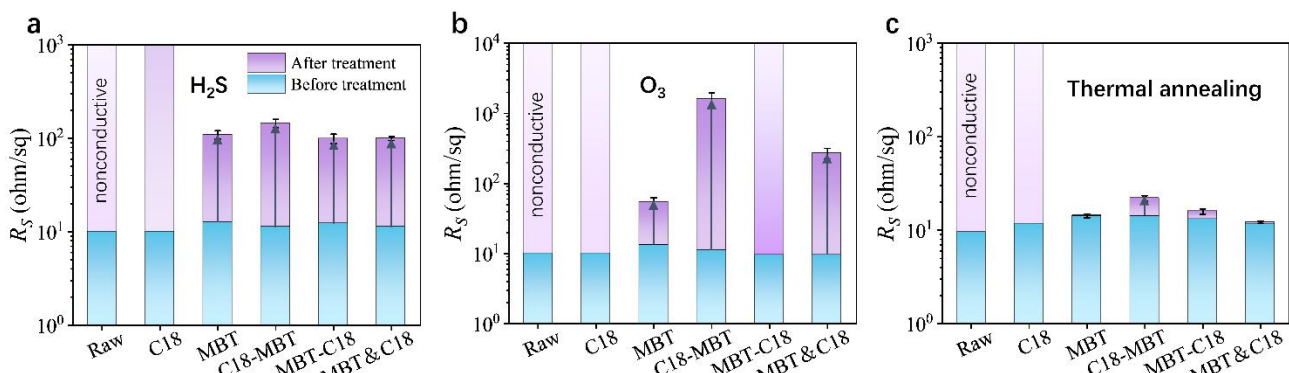


Figure S10. (a) Sulfidation, (b) oxidation, and (c) thermal annealing tests on raw AgNWs and the SAM-modified AgNWs. The gas concentrations of H_2S and O_3 are 150k ppm (2 hours) and 100k ppm (30 min), respectively. The annealing temperature is 280 °C for 1 hour.

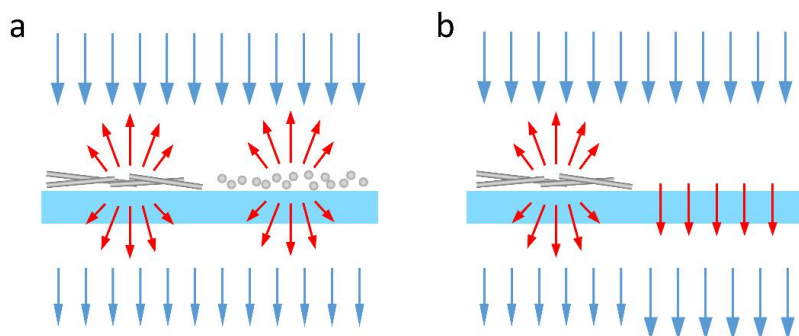


Figure S11. Schematic of the optical visibility for the (a) PRI-induced and (b) etched/removed AgNW patterns.

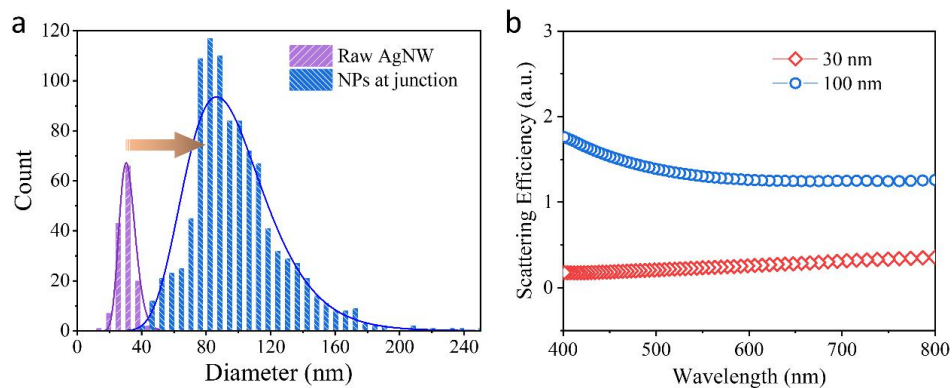


Figure S12. (a) Diameter statistics of the raw AgNWs and nanoparticles (NPs) formed at the junctions of the C18-AgNW network which has been annealed at 190 °C for 8 min. (b) Simulated scattering efficiency of individual nanowires with diameters of 30 and 100 nm.

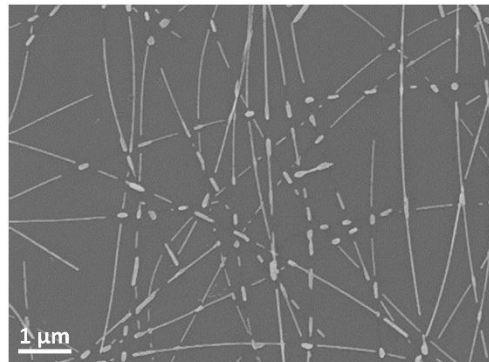


Figure S13. SEM image of the annealed C18-AgNW network with most breakdown at the junctions between NWs.

Table S1. Performance comparison of the AgNW-based heaters

Material	Diameter (nm)	Voltage (V)	Maximum Temperature (°C)	Ref
AgNW	/	5	275	[1]
AgNW	100	9	~80	[2]
NiO-AgNW	30	7	185	[3]
Ag-COOH/-NH ₂	60	8	175	[4]
AlOx-AgNW	30	7	81	[5]
AgNW	80	5.5	124	[6]
PEDOT:PSS/ITO-AgNW	35	11	115	[7]
GZO-AgNW-GZO-cPI	100	6	76	[8]
AgNW-PI	60-80	6	96	[9]
Ni-AgNW	40	30	284	[10]
FTO-NiCr-AgNW	50	7	193	[11]
UV polymer-AgNW	30	12	93.5	[12]
SWCNT-AgNW	40	16	182	[13]
Conductive polymer-AgNW	35	20	~200	[14]
TiO ₂ -AgNW	53	7	235	[15]
Welded-AgNW	30	6	145	[16]
ANFs-AgNW	40	2.5	~260	[17]
rGO-AgNW	350	-	458	[18]
PDMS-AgNW	90	2	160	[19]
MBT-AgNW	30	7	319	Our work

REFERENCES

- [1] Ergun, O.; Coskun, S.; Yusufoglu, Y.; Unalan, H. E. High-performance, bare silver nanowire network transparent heaters. *Nanotechnology* **2016**, *27*, 445708.
- [2] Won, P.; Park, J. J.; Lee, T.; Ha, I.; Han, S.; Choi, M.; Lee, J.; Hong, S.; Cho, K.-J.; Ko, S. H. Stretchable and Transparent Kirigami Conductor of Nanowire Percolation Network for Electronic Skin Applications. *Nano Lett.* **2019**, *19*, 6087-6096.
- [3] Patel, M.; Chauhan, K. R.; Kim, J.; Kim, J.-W.; Lim, D. AgNWs networks for high-performing transparent heaters by using NiO window layer. *Sensor. Actuat. A Phys.* **2017**, *267*, 8-13.
- [4] Oytun, F.; Alpturk, O.; Basarir, F. Coupling layer-by-layer assembly and multilayer transfer to fabricate flexible transparent film heater. *Mater. Res. Bull.* **2019**, *112*, 53-60.
- [5] Lee, J.-M.; Kim, Y.-H.; Kim, H.-K.; Kim, H.-J.; Hong, C.-H. Effect of AlOx protection layer on AgNWs for flexible transparent heater. *Sci. Rep.* **2020**, *10*, 4592.
- [6] Yan, X.; Li, X.; Zhou, L.; Chu, X.; Yang, F.; Chi, Y.; Yang, X. Electrically sintered silver nanowire networks for use as transparent electrodes and heaters. *Mater. Res. Express* **2019**, *6*, 116316.
- [7] Park, J.; Han, D.; Choi, S.; Kim, Y.; Kwak, J. Flexible transparent film heaters using a ternary composite of silver nanowire, conducting polymer, and conductive oxide. *RSC Adv.* **2019**, *9*, 5731-5737.
- [8] Wang, R.; Cai, P.; Xu, W.; Tan, R.; Shen, W.; Wang, Z.; Chen, G.; Huang, J.; Fang, X.; Song, W. Highly flexible and transparent film heaters based on colorless polyimide substrate with a GZO/AgNW/GZO sandwich structure. *J. Mater. Sci.: Mater. Electron.* **2020**, *31*, 4743-4751.
- [9] Huang, Q.; Shen, W.; Fang, X.; Chen, G.; Guo, J.; Xu, W.; Tan, R.; Song, W. Highly flexible and transparent film heaters based on polyimide films embedded with silver nanowires. *RSC Adv.* **2015**, *5*, 45836-45842.
- [10] Zhang, L.; Chen, Y.; Xu, C.; Liu, Z.; Qiu, Y. Nickel-enhanced silver nanowire-based transparent heater with large size. *RSC Adv.* **2018**, *8*, 14532-14538.
- [11] Kim, A. Y.; Kim, M. K.; Hudaya, C.; Park, J. H.; Byun, D.; Lim, J. C.; Lee, J. K. Oxidation-resistant hybrid metal oxides/metal nanodots/silver nanowires for high performance flexible transparent heaters. *Nanoscale* **2016**, *8*, 3307-3313.
- [12] Yang, H.; Bai, S.; Guo, X.; Wang, H. Robust and smooth UV-curable layer overcoated AgNW flexible transparent conductor for EMI shielding and film heater. *Appl. Surf. Sci.* **2019**, *483*, 888-894.
- [13] Goak, J. C.; Kim, T. Y.; Kim, D. U.; Chang, K. S.; Lee, C. S.; Lee, N. Stable heating performance of carbon nanotube/silver nanowire transparent heaters. *Appl. Surf. Sci.* **2020**, *510*, 145445.
- [14] Pyo, K.-h.; Kim, J.-W. Transparent and mechanically robust flexible heater based on compositing of Ag nanowires and conductive polymer. *Compos. Sci. Technol.* **2016**, *133*, 7-14.
- [15] Lagrange, M.; Sannicolo, T.; Muñoz-Rojas, D.; Lohan, B. G.; Khan, A.; Anikin, M.; Jiménez, C.; Bruckert, F.; Bréchet, Y.; Bellet, D. Understanding the mechanisms leading to failure in metallic nanowire-based transparent heaters, and solution for stability enhancement. *Nanotechnology* **2016**, *28*, 055709.

- [16] Huang, Y.; Tian, Y.; Hang, C.; Liu, Y.; Wang, S.; Qi, M.; Zhang, H.; Zhao, J. Self-Limited Nanosoldering of Silver Nanowires for High-Performance Flexible Transparent Heaters. *ACS Appl. Mater. Inter.* **2019**, *11*, 21850-21858.
- [17] Ma, Z.; Kang, S.; Ma, J.; Shao, L.; Wei, A.; Liang, C.; Gu, J.; Yang, B.; Dong, D.; Wei, L.; Ji, Z. High-Performance and Rapid-Response Electrical Heaters Based on Ultraflexible, Heat-Resistant, and Mechanically Strong Aramid Nanofiber/Ag Nanowire Nanocomposite Papers. *ACS Nano* **2019**, *13*, 7578-7590.
- [18] Yang, Y.; Chen, S.; Li, W.; Li, P.; Ma, J.; Li, B.; Zhao, X.; Ju, Z.; Chang, H.; Xiao, L.; Xu, H.; Liu, Y. Reduced Graphene Oxide Conformally Wrapped Silver Nanowire Networks for Flexible Transparent Heating and Electromagnetic Interference Shielding. *ACS Nano* **2020**, *14*, 8754-8765.
- [19] Yao, S.; Cui, J.; Cui, Z.; Zhu, Y. Soft electrothermal actuators using silver nanowire heaters. *Nanoscale* **2017**, *9*, 3797-3805.